A Comparative Study on the Impact of Preparation Technique on the Minority Carrier Lifetime of Cu2O Absorber

Chithira Venugopalan Kartha, Yi-Teng Huang, Theodoros Dimopoulos, Stefan Edinger, Dominique Muller, Stéphane Roques, Jérémy Bartringer, Abdelilah Slaoui, Robert L. Z. Hoye, Thomas Fix

A Comparative Study on the Impact of Preparation Technique on the Minority Carrier Lifetime of Cu_2O Absorber

Chithira Venugopalan Kartha *[a], *Yi-Teng Huang* [b,c], *Theodoros Dimopoulos* [d], *Stefan Edinger* [d], *Dominique Muller* [a], *Stéphane Roques* [a], *Jérémy Bartringer* [a], *Abdelilah Slaoui* [a], *Robert L.Z. Hoye* [c], *Thomas Fix* [a]

[a] ICube laboratory, Université de Strasbourg and CNRS, 23 rue du Loess, BP 20 CR, F-67037 Cedex 2 Strasbourg, France

[b] Cavendish Laboratory, University of Cambridge, JJ Thomson Ave, Cambridge CB3 0HE, United Kingdom

[c] Inorganic Chemistry Laboratory, Department of Chemistry, University of Oxford, South Parks Road, Oxford OX1 3QR, United Kingdom

[d] Power and Renewable Gas Systems, Center for Energy, AIT Austrian Institute of Technology, Giefinggase 4, 1210 Vienna, Austria

[*]Email: kartha.chithira@gmail.com

ABSTRACT:

Cu_2O solar cells are attractive but still provide conversion efficiencies well below their theoretical limits. In this work we compare the charge-carrier dynamics of Cu_2O absorbers prepared using the popular techniques of Magnetron Sputtering, Electrodeposition, Pulsed Laser Deposition (PLD) and Thermal Oxidation. This is performed using Transient Absorption (TA) spectroscopy and Time-resolved Photoluminescence (TRPL). All samples after optimization show an average carrier lifetime in the ns range. The electrodeposited samples provide the highest value. This work should stimulate the use of carrier lifetime techniques for the optimization of Cu_2O absorbers.

KEYWORDS: Pulsed Laser Deposition, Magnetron Sputtering, Electrodeposition, Cu_2O, Solar Cell, TRPL

1. INTRODUCTION

Among oxide photovoltaic absorbers, Cu_2O is one of the most promising materials. Apart from its abundance and non-toxicity, Cu_2O also has a high absorption coefficient above 10^5 cm^{-1} in the visible region of the solar spectrum[1] and a favorable direct bandgap of 1.9-2.2 eV which makes it attractive for photovoltaic applications. However, the achieved power conversion efficiency with Cu_2O solar cells till date is below 10 %, which is way below its Shockley-Queisser Limit (~ 20 %)[2, 3]. There have been numerous efforts to improve the efficiency with Cu_2O absorbers since photoelectric effect was first discovered in this oxide in the 1930s. One of the main challenges is the low stability of Cu_2O at room temperature and hence obtaining only Cu_2O phase without any parasitic CuO is very tricky. Additionally, for heterojunction solar cells, a proper band alignment and reduction of interface defects are also key factors for improving the efficiency.

The conductivity of Cu_2O is mainly from Cu vacancies that depend on the temperature and pressure conditions during their synthesis. Hence, it is important to deeply understand the Cu_2O absorbers grown via different techniques to improve their photovoltaic performance. Cu_2O absorbers can be prepared via both chemical[4–6] and physical processes[7–9]. However, the widely used preparation techniques are electrodeposition[10–14], magnetron sputtering[15–19] and thermal oxidation[20–23]. Cu_2O solar cells with absorbers prepared via thermal oxidation of Cu sheets are by far the most efficient solar cells reported in literature[24–26]. However, there is a huge diversity in the reported efficiencies with Cu_2O absorbers prepared via similar techniques[27, 28]. Since

thermal oxidation of copper sheets involves very high temperature (above 1000 ℃), alternative techniques for the growth of high performing Cu_2O absorber are necessary for large scale applications especially when employing flexible substrates. There are only few reports on Pulsed Laser Deposited (PLD)[29–32] and Atomic Layer Deposited (ALD)[33, 34] Cu_2O in the literature, and none of the solar cells based on these absorbers have shown improved efficiencies.

Understanding the carrier lifetime is crucial in the application of Cu_2O as an absorber as longer minority carrier lifetimes are beneficial for charge extraction. However, there are not many experimental reports on carrier lifetime analysis on Cu_2O thin films[35]. A detailed understanding of the impact of preparation techniques on the minority carrier lifetimes is thus essential when choosing the Cu_2O absorber preparation technique.

In this work, we have compared the properties of Cu_2O absorbers prepared using the popular techniques of magnetron sputtering, electrodeposition, PLD and thermal oxidation to better understand the impact of the preparation technique on the quality of Cu_2O which in turn influences its absorber properties. We report the results of advanced transient measurements on these absorbers prepared via the four different techniques to identify their carrier lifetimes and defects, which to the best of our knowledge was not studied before. This work can help to correlate the surface quality and carrier transport properties in Cu_2O when grown via different techniques.

2. EXPERIMENTAL DETAILS

Cu_2O Absorber Preparation

Pulsed Laser Deposition: The PLD Cu_2O absorber was prepared using the conditions previously described in Kartha et al[29]. The deposition was carried out on quartz substrate (1.5 x1.5 cm^2) at a temperature of 750 ℃ and an oxygen partial pressure of 10^{-2} mbar using a CuO target. After deposition the sample was naturally cooled down to room temperature in the same atmosphere.

RF Magnetron Sputtering: For the deposition of Cu_2O films via RF magnetron sputtering, a high purity (99.99+ %) Cu target from Goodfellow was used. Target-Substrate distance was fixed at 25 cm, and the deposition was carried out at 300 ℃ at 53 W power and an oxygen flow rate of 1.8 sccm. The Argon flow rate was fixed at 16 sccm and sputtering pressure at 3.4 mTorr. Approximately 100 nm thick film was sputtered on quartz substrate (1.5 x1.5 cm^2) for the studies.

Electrodeposition: For the electrodeposition, ITO-coated glass (from Sigma-Aldrich), with a sheet resistance of 8-12 Ohm/sq. was used as the substrate (2.5 x2.5 cm^2). For the electrodeposition solution, 0.2 M Cu sulfate pentahydrate ($CuSO_4 \times 5H_2O$, Sigma C8027) were dissolved in 3 M lactic acid ($C_3H_6O_3$, Sigma, W261114) and stirred constantly in a water bath for cooling. Highly concentrated NaOH solution (NaOH pellets, Sigma S5881) was slowly added to the mixture, bringing the pH to the final value of 12.5. The total thickness of the Cu_2O was 2.5 µm determined from the total charge that has flown in the cell over time [11].

Thermal Oxidation: Thermally oxidized Cu_2O sheet was obtained using 0.127 mm thick laminated copper foils (99.9% purity) from Alfa Aesar as the starting material. The oxidation process was carried out at 1050 ℃ at an oxygen concentration of 10,000 ppm for one hour in the presence of Argon.

Cu_2O Absorber Characterization

The stoichiometric Cu_2O phase of all the samples considered in this study was confirmed using X-ray diffraction studies. A Rigaku Smartlab diffractometer equipped with a monochromatic source delivering a Cu $K\alpha_1$ incident beam (45 kV, 200 mA, 0.154056 nm) and Bruker-AXS D8 Advance X-ray diffractometer with $CuK\alpha_1$ radiation (λ = 0.154056 nm) were used for the same. For completeness on films composition, a Horiba LabRAM ARAMIS Raman spectrometer with 532 nm laser excitation was used to study the Raman footprints of the deposited films. For the long time TA measurements, the third harmonic of 355 nm pump pulses was provided by an electronically controlled, Q-switched Nd:YVO_4 laser (Innolas Picolo 25) with a pump width ~800 ps passing through several non-linear crystals equipped. For the short-time TA, the second harmonic of 400 nm pump pulses was created from a Ti:Sapphire laser (Solstice Ace) with pump width ~100 fs passing through a beta barium borate crystal (Eksma Optics). Broadband probe pulses with wavelength ~400 – 600 nm were generated by focusing an 800 nm wavelength fundamental laser onto a CaF_2 crystal (Eksma Optics, 5mm) controlled by a digital motion controller (Mercury C-863 DC Motor Controller). The short-time measurements could be taken in transmission (TA) or reflection (TR) configuration depending on the samples and substrates. The repetition rate of the pump pulses was initially 1 kHz, but the reflection/transmittance probe pulses from the samples with or without pump excitation ($T_{pump\ on}$, $T_{pump\ off}/R_{pump\ on}$, $R_{pump\ off}$) were collected at a rate of 500 Hz, which was controlled by a rotating chopper wheel. The

reflected/transmitted pulses were collected by a monochrome line scan camera (JAI SW-4000M-PMCL; spectrograph, Andor Shamrock SR-163). These reflections/transmittances were used to calculate the TA/TR signal intensity by $\frac{\Delta R}{R} = \frac{R_{pump\ on} - R_{pump\ off}}{R_{pump\ off}}$ and $\frac{\Delta T}{T} = \frac{T_{pump\ on} - T_{pump\ off}}{T_{pump\ off}}$, respectively.

To compare the PL kinetics of the Cu_2O, two techniques were followed namely Time Resolved Photoluminescence (TRPL) and Time-Correlated Single Photon counting (TCSPC). TRPL is a powerful technique to investigate the decay of radiative recombination pathways of the charge carriers. A pulsed laser excites the charge carriers in a sample and the subsequent decay of the photoluminescence is measured as a function of time. For the measurement, an Andor iStar DH740 CCI-010 system connected to a grating spectrometer (Andor SR303i) was used at the Cambridge University. An excitation wavelength of 400 nm was used to measure the photoluminescence spectrum of the sample and an intensified charge-coupled device (ICCD) camera was used to provide time and spectral resolution. The time-resolution of the ICCD camera was only 4 ns. Using TRPL, radiative recombination events only > 1 ns after excitation could be measured. So, for a better time resolution, TCSPC technique was also followed which has a time resolution of ~ 20 ps. TCSPC measurements were taken in the Edinburgh Instruments Life Spec system, FLS1000. A picosecond pulsed (~80 ps) diode laser (EPL-405, Edinburgh Instruments), with a wavelength of 405 nm was used for the excitation. The repetition rate was set at 40 kHz during the measurements.

Solar cell fabrication methods are described in [11, 29] and do not constitute the main focus of the present work.

3. RESULTS AND DISCUSSION

The phase of the deposited absorbers was confirmed with the help of X-ray diffraction. Grazing angle (3°) XRD measurement was taken for the PLD, sputtered and electrodeposited films to maximize signal from polycrystalline films in respect to the underlying substrates. As shown in Figure 1 all samples were phase-pure Cu_2O, without any detectable CuO phases. The sputtered, electrodeposited and thermally oxidized samples were (111)-axis oriented, whereas the PLD Cu_2O sample had (2 0 0) preferred orientation. Film texture is influenced among others by the deposition method, ion bombardment and also by deposition temperature.

The fabrication temperature of the different Cu_2O films or foils varies depending on the technique used. PLD films are grown at 750 °C, sputtering films at 300 °C, electrodeposited films at 50-80 °C, and thermally oxidized foils at 1050 °C. This range of temperatures specific for each technique is commonly used for Cu_2O and provides the best quality in terms of phase purity as demonstrated by XRD (Figure 1) and Raman spectroscopy (Figure S1) where no presence of parasitic CuO could be detected. For PLD, deposition temperature has been optimized in previous work from room temperature to 800°C [29] and the temperature of 750 °C was selected from this study to obtain the best quality films.

As we will discuss next the fact that the deposition technique and temperature are varied induces different stress levels in the films. However there is little impact of stress on the bandgap which is around 1.97 eV for PLD, sputtering and thermally oxidized samples as determined from photoluminescence.

PLD films are grown at 750 °C, a much higher temperature than the sputtering growth at 300°C which can lead to different texture properties. The lattice parameters of the films calculated from the diffraction peaks revealed a lattice constant close to pure Cu_2O (4.267 Å JCPS:01-078-2076) for the PLD and electrodeposited films and the thermally oxidized sheet as can be seen in **Table *1*** while the sputtered Cu_2O film had a deviation of 0.6% from the lattice constant of pure Cu_2O. The oxidized foils showed a higher mean grain size of 109 nm calculated from the Scherrer´s equation[36] which is seven times higher than the mean grain size of the Cu_2O films prepared via PLD, sputtering and electrodeposition. Increase in grain size decreases recombination and scattering at grain boundaries, improving the overall electrical properties of the absorber. The stress is calculated from the XRD data using the following equation[37, 38]:

$$\sigma = \frac{-E\,(a - a_0)}{2\upsilon a_0}$$

where E is the Young's Modulous of Cu_2O (30 GPa), a_0 is the lattice parameter of the bulk, a is the measured lattice parameter of the film and υ is the Poisson's ratio of Cu_2O (0.45).

The PLD, sputtering and electrodeposited films have tensile stress while the thermal oxidation sample has compressive stress (Table 1). The sputtered film was found to have higher stress than the rest of the Cu_2O absorbers. This can be observed in the shift of the interplanar spacing in Figure 1, resulting in an increase of the lattice constant as shown in Table 1.

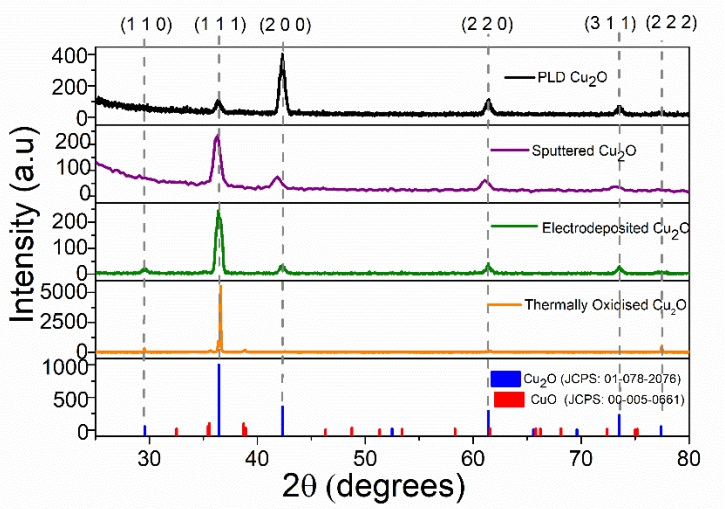

Fig. 1 Grazing angle X-ray diffractogram ($CuK_{\alpha 1}$ radiation ($\lambda = 0.154056$ nm) of the Cu_2O absorbers prepared via PLD, sputtering and electrodeposition and θ-2θ diffraction peaks of thermally oxidized Cu_2O sheet compared to the reference of Cu_2O and CuO from the ICCD database

Table 1 Lattice Parameters, grain size and stress calculated from X-ray diffraction peaks

Preparation Method	Lattice Constant (Å)	Mean Grain size (nm)	Stress (GPa)
PLD	4.269	15	0.01
Sputtering	4.294	10	0.21
Electrodeposition	4.268	12	0.007
Thermal Oxidation	4.258	109	-0.07

Understanding the carrier dynamics is critical when employing a material as a photovoltaic absorber. Longer lifetime of the excitonic state is favorable for the efficient charge separation before their loss via recombination. Comparing the lifetime of the excited states in Cu_2O films prepared via different techniques will thus help in better understanding their potential as photovoltaic absorbers. The carrier dynamics of the films in this study was analyzed using several advanced techniques. As the lifetime of excitonic states is short-lived, i.e. typically in the ns time range, transient absorption (TA) spectroscopy is a reliable technique to measure it. As can be seen

in Figure 2(a), the transient absorption peak of the PLD Cu_2O film has three visible spectra regions. A ground state bleach (GSB) at ~ 2.17 eV in the spectral region of 570-575 nm, and two photo induced absorption (PIA) peaks at ~2.19 eV (562-567 nm) and ~2.03 eV (605-615 nm), respectively. The PIA could be from ortho-exciton state or absorption from copper interstitial to conduction band sub-band (C2) [34]. Carrying out an exponential fit of the peak kinetics, both peaks were found to have very fast decay times (< 1ps). Both the GSB and PIA dips showed exponential decay. The decay time of the GSB peak was 355 *f*s and PIA decayed at 883 *f*s and 364 *f*s when fitted with an exponential function as can be seen in Figure 2(b). However, comparing with the sputtered Cu_2O, apart from having multiple peaks (two GSB signals at 420-460 nm and 600-690 nm and two PIA signals at 460-500 nm and 690-740 nm) a much longer exciton lifetime was observed in the sputtered film as can be seen in Figure 2(c) with PIA peaks not decayed even at 1000 ps (1 ns). The multiple peaks in the sputtered film could be due to energy states induced by the presence of copper vacancies or interstitials within the bandgap of the film. Upon fitting the GSB peak (420-460 nm) with a bi-exponential decay function, a much larger time constant in the range of ps (0.96 ps and 137.16 ps) was observed (Figure 2(d)). Figure 2(d) also shows the kinetics at different pump fluences, which is found to have little influence. Additionally, the PIA signal was also found to have a longer lifetime as the signal did not decay even at 1 ns (Figure S2(c)). The fast decay in the PLD film could be due to the presence of defects or trap states. Similar lifetime was observed in oxidized Cu_2O reported by Shenje et.al[35]. Azimi et.al[39] have also reported a decay time of 0.5 ps ±0.06 for Cu_2O nanoparticles prepared via chemical treatment and have explained it to be the exciton lifetime which decays fast due to the presence of defect or trap states.

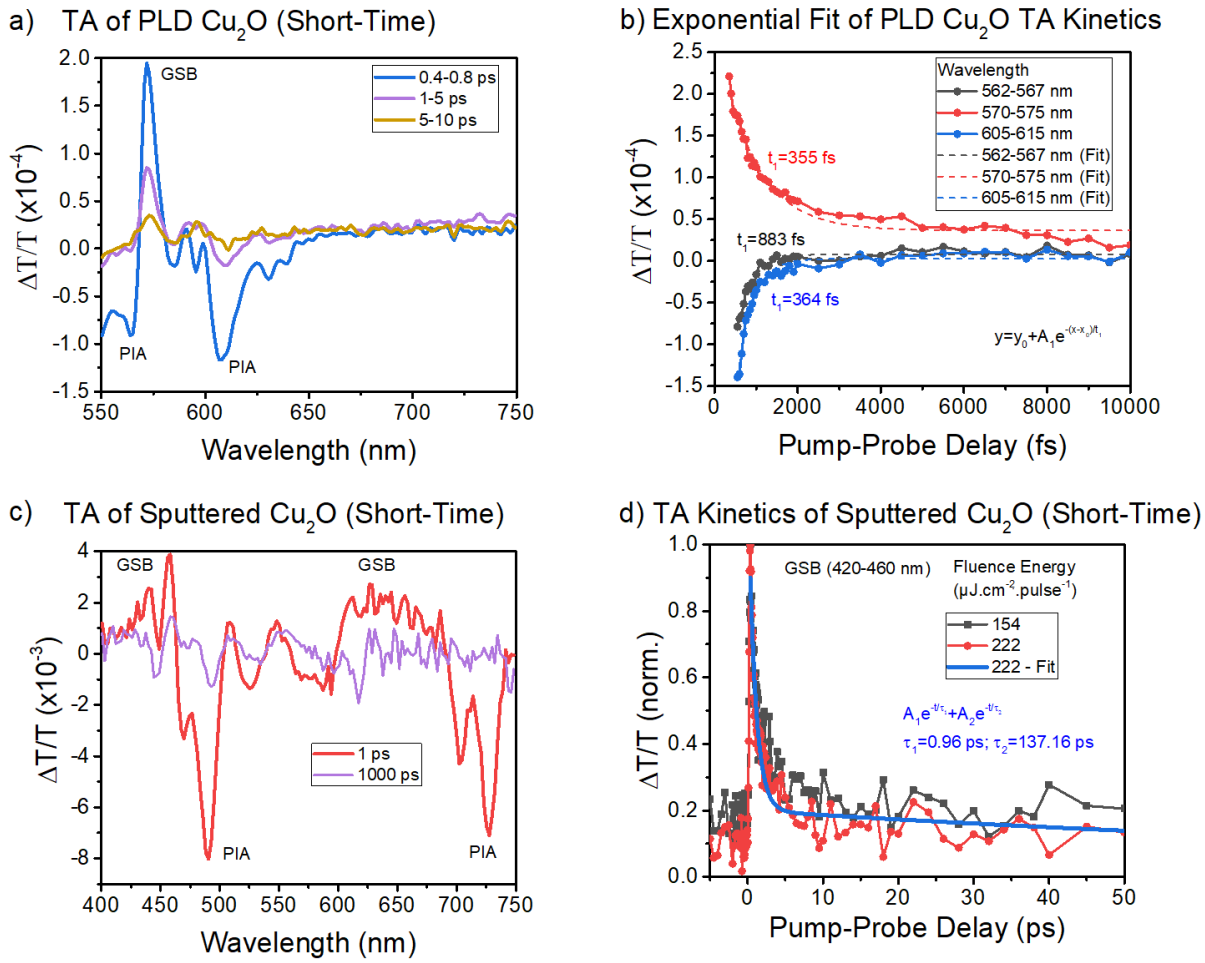

Fig. 2 (a) Transient Absorption spectrum, exponential fit of the transient absorption peaks and dips with the fitting equation for (a,b) PLD Cu_2O (laser at 460 nm with 40μW) (c,d) sputtered Cu_2O (pump wavelength 400 nm).

During the measurement of long-time TA of the PLD film, at 355 nm excitation wavelength and power of 400 μW, an unknown long lifetime component with a negative feature was observed at an energy state larger than the bandgap (Figure S2(a)). The TA kinetics of this feature at a wavelength of 540 nm (Figure S2(b)) was fitted by an exponential decay function with a rather longer decay time of ~ 20 ns. Azimi et.al[39] have also observed a similar long lifetime component which was stable beyond their experimental window of 8 ns which they attribute to a trap state, which lowers the lifetime of the excitonic state. In our PLD Cu_2O film, the kinetics of the TA signal was independent of fluences. This could be due to a trap state which is affecting excitonic transition lifetimes, which was not observed in the sputtered film (Figure S2(c)). Transient reflectivity measurements were taken on the electrodeposited Cu_2O samples because they are non-transparent. They revealed stronger GSB signal (480-540 nm) which was not found to decay within 10 ps, while

for the PLD and sputtered film all the signals (both GSB and PIA) decay within 10 ps as can be seen in Figure 3. This could point toward a better carrier lifetime of the electrodeposited film compared to the PLD and sputtered Cu_2O. While the negative peaks at 445-465 nm are present in the three samples and originate from band-to-band / exciton transitions, the positive peak at 440 nm corresponds to the indigo exciton peak (E_{OD} edge as described in [40]) and is visible only in the PLD sample, indicating a different surface quality.

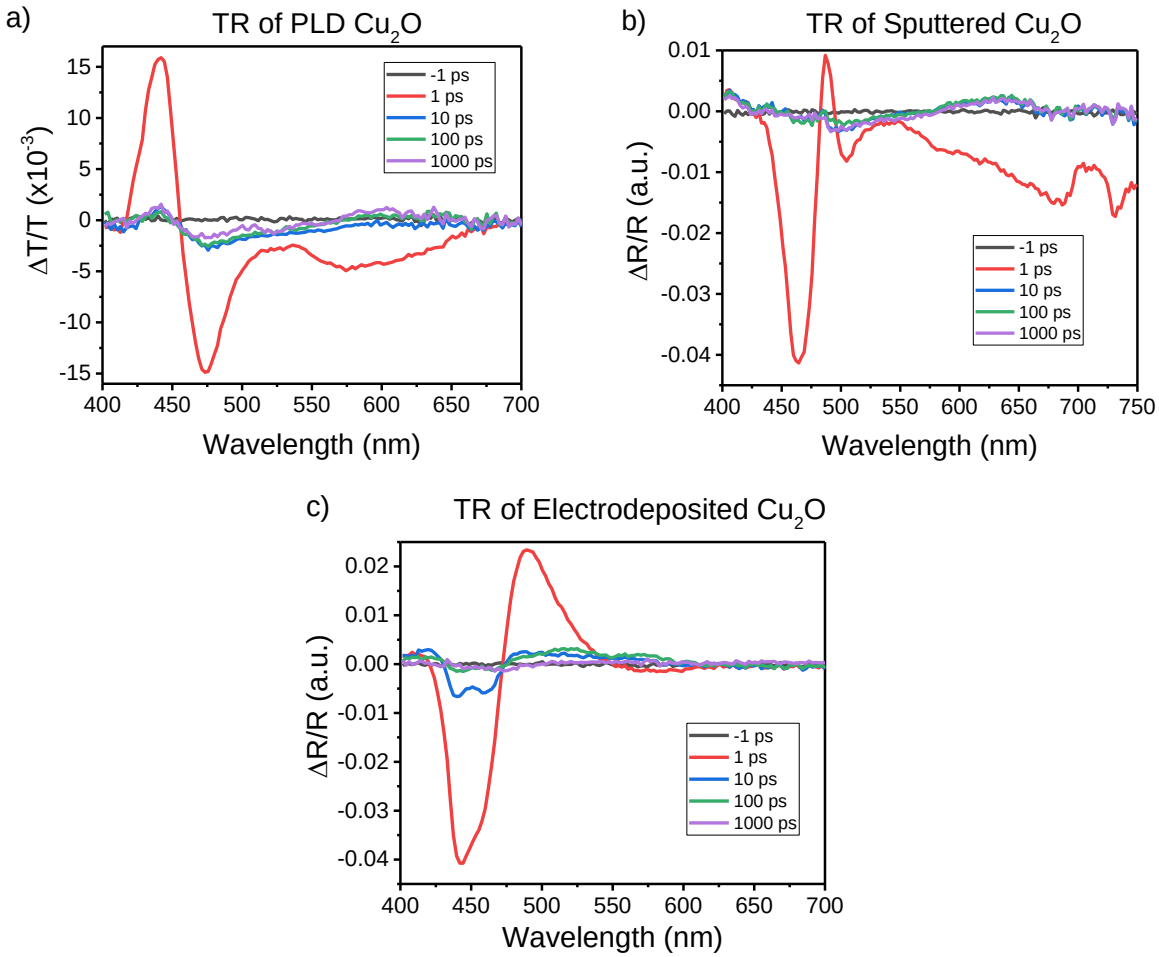

Fig. 3 Time dependent TR spectrum of (a) PLD (b) sputtered (c) electrodeposited Cu_2O

As the presence of sub-bandgap states could be a reason affecting the carrier lifetime in disordered absorbers and since it is hard to determine them from transmittance or reflectivity measurements, a highly sensitive technique of Photothermal Deflection Spectroscopy (PDS) was carried out. The optical bandgap estimated from Tauc-plot for the PLD, and sputtered film was 2.1 eV and 2.3 eV respectively. In the PDS measurement of the PLD and sputtered Cu_2O film, a non-zero absorbance

below their bandgap was found for both the films as can be seen in Figure 4(b) (the dashed lines indicate the onset of main absorption). However, for the sputtered Cu_2O, the absorbance onset is not sharp around the bandgap and higher absorbance than the PLD film below the bandgap can be seen which could be due to higher sub-gap states in the sputtered Cu_2O film. The presence of sub-gap states is not favoured as they lead to recombination pathways in an absorber. For the PLD film a sharp absorbance onset around its bandgap is visible. Hence comparing both the films, the PLD film might have lower sub-gap defects than sputtered film. In the TA spectroscopy of the PLD film, the long lifetime component was observed at higher energies from the bandgap. This result from the PDS further points that the poor performance of the PLD film might not be only due to sub-gap defects or traps as it is much lower for PLD Cu_2O than for the sputtered Cu_2O.

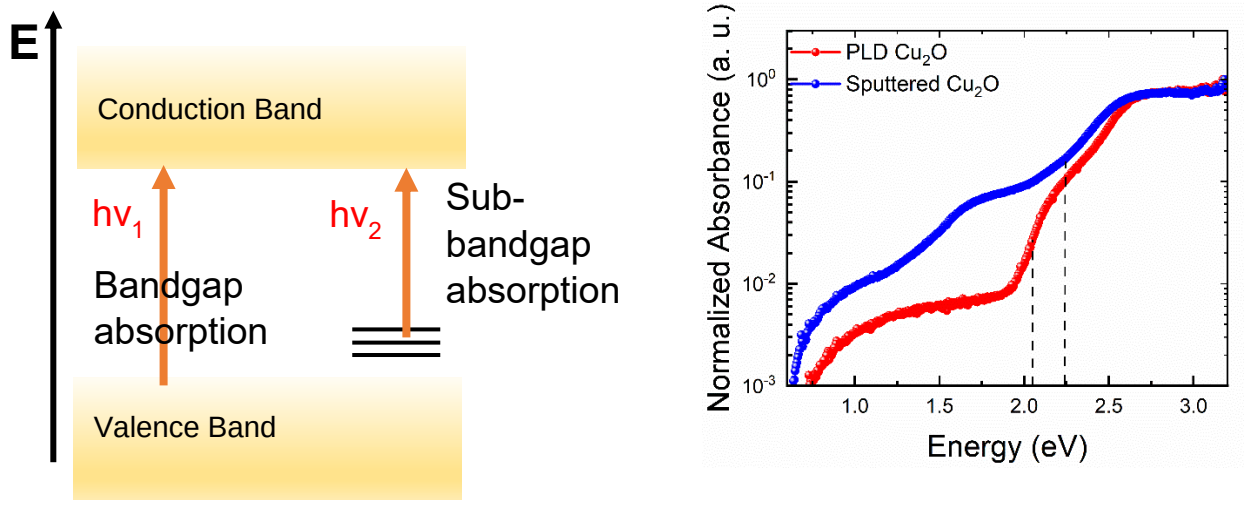

(a) (b)

Fig. 4 (a) Absorption edge and sub-band gap states in disordered absorbers (b) Normalized absorbance spectra of PLD and sputtered Cu_2O measured from PDS (Dashed lines mark the onset of main absorption)

Fitting the band-edge transition exciton peak decay in PL kinetics also helps to have an idea on the influence of defects on the charge carrier lifetimes. However, the time resolution of the TRPL setup is roughly 4-5 ns (Figure S3). In the TRPL spectrum of the sputtered Cu_2O at 400 nm excitation wavelength, emission peaks at 725 nm are visible apart from the band edge transition (626 nm) at energies smaller than the bandgap which could correspond to trap states namely copper vacancy and copper interstitials (Figure S3). This confirms the sub-bandgap absorption observed in the

sputtered film from PDS. All the PL peaks were found to decay within 15 ns which is fast but was better than the PLD film (315 ps as shown later). However, the sputtered film did not give a signal in Time-Correlated Single Photon-Counting (TCSPC) measurements, which could be due to the weaker laser diode excitation source used than for TRPL. To better understand the PL kinetics with better time resolution, TCSPC measurement was taken in all the other samples. The PL kinetics required fitting with multiple exponential functions suggesting the presence of parallel paths of photocarrier loss. PL kinetics was fitted using a biexponential function for the PLD film as shown in Figure 5(a). Fitting with exponential functions allows to determine lifetime values. There were two decay components with a smaller lifetime of 0.05 ns and a longer lifetime of 0.58 ns. The average decay time which corresponds to the carrier lifetime was found to be ~ 315 ps. A similar fast decay of the photogenerated carriers was also reported by Li et.al[41] in TRPL measurements of Cu_2O nanocrystals prepared via chemical route. This fast decay time is not favorable when employing these films as absorbers as the excited carriers are lost much faster via radiative recombination. The band edge emission was observed at a higher wavelength of 585 nm corresponding to a bandgap of 2.1 eV in thermally oxidized Cu_2O (Figure S4). As Cu_2O has a bandgap of 2.1 eV, the PL emissions might be due to contribution of defect states or from surface states other than the recombination of electron from conduction band to valence band. The decay profiles follow a tri-exponential decay with average decay times of 3.83 ns (for 585 nm peak). A peak at 476 nm was also observed which could be due to C2-V2 transition with a longer lifetime. The band structure of Cu_2O has 10 valence bands and 4 conduction bands; C2 and V2 correspond to the second lowest conduction band and the second highest valence band at the zone center[42]. The electrodeposited film had three peaks at 490 nm, 585 nm and 625 nm. The peak at 490 nm had the longest lifetime in the PL kinetics and is more likely from band-band transition while the other PL peaks could be from defect transitions and thus with shorter lifetime.

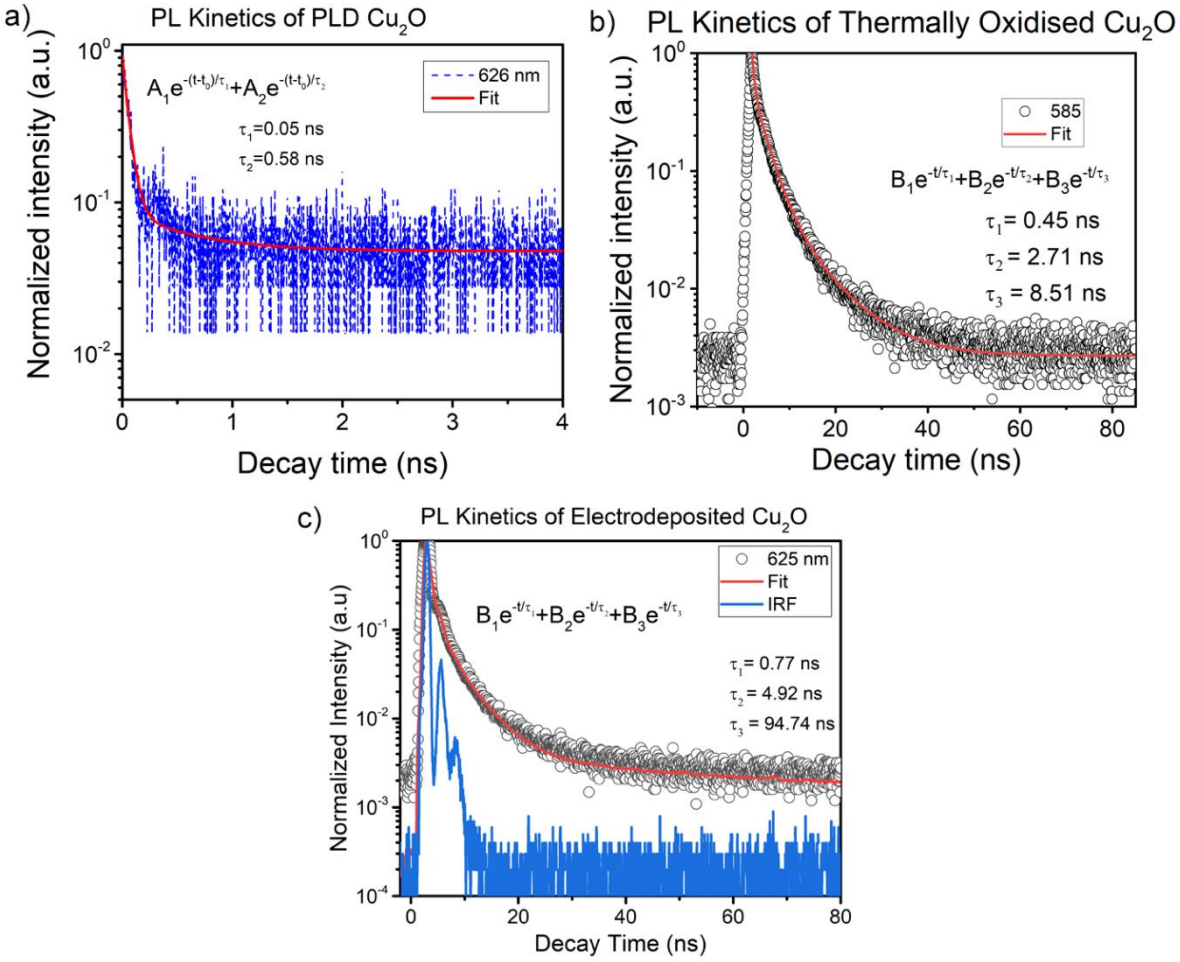

Fig. 5 (a) PL kinetics of the exciton peak at 626 nm of PLD Cu_2O with its bi-exponential fit (b) Kinetics of the PL peaks at 585 nm of thermally oxidized Cu_2O with a tri-exponential fit (c) PL kinetics of the exciton peak at 625 nm of Electrodeposited Cu_2O with a tri-exponential fit

Table 2 summarizes the PL decay time in Cu_2O absorbers prepared via different routes. Hossain et.al[12] have reported a lifetime of less than 1 ns for the electrodeposited Cu_2O which is in agreement with the τ_1 value found of 1.88 ns. The decay time for thermally oxidized Cu_2O sheets and electrodeposited films is much longer than the PLD Cu_2O, which means that the minority carrier lifetime is better and the charge separation in the absorber is more efficient.

Table 2 Average carrier lifetime measured from PL Kinetics

Sample	PL Analysis Technique	Time Constant (ns)
PLD Cu_2O	TCSPC	τ_1=0.05, τ_2=0.58
Sputtered Cu_2O	TRPL	<5
Electrodeposited Cu_2O	TCSPC	τ_1=1.88, τ_2=6.69, τ_3=44.27
Thermally Oxidized Cu_2O	TCSPC	τ_1=0.45, τ_2=2.71, τ_3=8.51

4. CONCLUSIONS

To conclude, in this work we have studied carrier lifetime of optimized Cu_2O films prepared by PLD, sputtering, electrodeposition and also thermally oxidized Cu_2O foils. We propose a comparison of Cu_2O fabricated and optimized by these four different techniques, spanning from material fabrication and optimization, advanced characterization including minority carrier lifetime, to device fabrication, using a similar methodology for all techniques. These are techniques commonly used for fabricating Cu_2O solar cells. The innovation of this work is to underline the relation between carrier lifetime and the efficiency of solar cells with Cu_2O absorbers fabricated by widely different techniques, spanning deposition temperatures from close to ambient to >1000°C. It is found that for all the Cu_2O samples a relatively short carrier lifetime is measured, while values higher by one or more orders of magnitude would be satisfactory for high quality photovoltaic absorber material as is the case for silicon. The τ_1 time constants from Table 2 obtained with the different techniques are reminded in Table 3. From this table it can be seen that despite the solar cell architectures are different because of fabrication constraints, the open circuit voltage and the conversion efficiency from the different fabrication methods are evolving in a logical way with respect to the average carrier lifetime measured from photoluminescence. The different current density vs. voltage curves are shown in Fig. S5 as well as the architectures.

This work should stimulate the use of PL kinetics measurements for the fabrication of Cu_2O solar cells that remains challenging but also full of opportunities for further improvement.

Table 3 Champion test solar cells characteristics and relation to average carrier lifetime

Preparation method of Cu_2O absorber	Solar cell architecture	Short circuit current density (mA/cm^2)	Open circuit voltage (V)	Fill factor (%)	Efficiency (%)	t_1 time constant (ns)
PLD	LSMO/Cu_2O/$Zn_{1-x}Ge_xO_4$/AZO	0.025	0.12	28	0.0008	0.05
Sputtering	AZO/Cu_2O/ITO	1.76	0.26	28	0.13	<5
Electrodeposition	AZO/Nb:TiO_2/ZnOS/ Cu_2O/ITO	4.02	0.28	27	0.30	1.88
Thermal oxidation	AZO/ZnO/Cu_2O/Au	1.90	0.19	25	0.09	0.45

ACKNOWLEDGEMENTS

The authors would like to acknowledge the contribution of M. Lenertz from the Institut de Physique et Chimie des Matériaux de Strasbourg (IPCMS) for the XRD analysis. The authors also wish to thank the staff from the C^3FAB platform of ICube laboratory and G. Ferblantier for sputtering.

This work was supported by Centre National de la Recherche Scientifique (CNRS) and University of Strasbourg. Y.-T.H. and R.L.Z.H. thank the Engineering and Physical Sciences Research Council (EPSRC) for funding (no. EP/V014498/2). R.L.Z.H. thanks the Royal Academy of Engineering for support through the Research Fellowships scheme (no. RF\201718\17101).

COMPETING INTERESTS

Authors declare that they have no known competing financial interests or personal relationships that could have appeared to influence the work reported in this paper.

SUPPLEMENTARY INFORMATION

Raman spectra; long time TA spectra; TRPL of PLD and sputtered Cu_2O; PL spectrum of thermally oxidized Cu_2O; current density vs. voltage of solar cell devices.

AUTHOR INFORMATION

Corresponding Author

Chithira Venugopalan Kartha

kartha.chithira@gmail.com

REFERENCES

1. Malerba C, Biccari F, Leonor Azanza Ricardo C, et al (2011) Absorption coefficient of bulk and thin film Cu2O. Solar Energy Materials and Solar Cells 95:2848–2854. https://doi.org/10.1016/j.solmat.2011.05.047

2. Shockley W, Queisser HJ (1961) Detailed Balance Limit of Efficiency of p-n Junction Solar Cells. Journal of Applied Physics 32:510–519. https://doi.org/10.1063/1.1736034

3. Sekkat A, Bellet D, Chichignoud G, et al (2022) Unveiling Key Limitations of ZnO/Cu2O All-Oxide Solar Cells through Numerical Simulations. ACS Appl Energy Mater 5:5423–5433. https://doi.org/10.1021/acsaem.1c03939

4. Ristov M, Sinadinovski G, Grozdanov I (1985) Chemical deposition of Cu2O thin films. Thin Solid Films 123:63–67. https://doi.org/10.1016/0040-6090(85)90041-0

5. Saadaldin N, Alsloum MN, Hussain N (2015) Preparing of Copper Oxides Thin Films by Chemical Bath Deposition (CBD) for Using in Environmental Application. Energy Procedia 74:1459–1465. https://doi.org/10.1016/j.egypro.2015.07.794

6. Laurie AB, Norton ML (1989) Preparation and characterization of thin films of copper(II) oxide by low temperature normal pressure metalorganic chemical vapor deposition. Materials Research Bulletin 24:213–219. https://doi.org/10.1016/0025-5408(89)90128-1

7. Chua D, Kim SB, Li K, Gordon R (2019) Low Temperature Chemical Vapor Deposition of Cuprous Oxide Thin Films Using a Copper(I) Amidinate Precursor. ACS Appl Energy Mater 2:7750–7756. https://doi.org/10.1021/acsaem.9b01683

8. Gupta N, Singh R, Wu F, et al (2013) Deposition and characterization of nanostructured Cu2O thin-film for potential photovoltaic applications. Journal of Materials Research 28:1740–1746. https://doi.org/10.1557/jmr.2013.150

9. Iivonen T, Heikkilä MJ, Popov G, et al (2019) Atomic Layer Deposition of Photoconductive Cu2O Thin Films. ACS Omega 4:11205–11214. https://doi.org/10.1021/acsomega.9b01351

10. De Jongh P, Vanmaekelbergh D, Kelly J (1999) Cu2O: electrodeposition and characterization. Chemistry of materials 11:3512–3517

11. Kaur J, Bethge O, Wibowo RA, et al (2017) All-oxide solar cells based on electrodeposited Cu2O absorber and atomic layer deposited ZnMgO on precious-metal-free electrode. Solar Energy Materials and Solar Cells 161:449–459. https://doi.org/10.1016/j.solmat.2016.12.017

12. Hossain MdA, Al-Gaashani R, Hamoudi H, et al (2017) Controlled growth of Cu 2 O thin films by electrodeposition approach. Materials Science in Semiconductor Processing 63:203–211. https://doi.org/10.1016/j.mssp.2017.02.012

13. Tran MH, Cho JY, Sinha S, et al (2018) Cu2O/ZnO heterojunction thin-film solar cells: the effect of electrodeposition condition and thickness of Cu2O. Thin Solid Films 661:132–136. https://doi.org/10.1016/j.tsf.2018.07.023

14. Jeong SS, Mittiga A, Salza E, et al (2008) Electrodeposited ZnO/Cu2O heterojunction solar cells. Electrochimica Acta 53:2226–2231. https://doi.org/10.1016/j.electacta.2007.09.030

15. Zhu H, Zhang J, Li C, et al (2009) Cu2O thin films deposited by reactive direct current magnetron sputtering. Thin Solid Films 517:5700–5704. https://doi.org/10.1016/j.tsf.2009.02.127

16. Dolai S, Das S, Hussain S, et al (2017) Cuprous oxide (Cu2O) thin films prepared by reactive d.c. sputtering technique. Vacuum 141:296–306. https://doi.org/10.1016/j.vacuum.2017.04.033

17. Zhang L, McMillon L, McNatt J (2013) Gas-dependent bandgap and electrical conductivity of Cu2O thin films. Solar Energy Materials and Solar Cells 108:230–234. https://doi.org/10.1016/j.solmat.2012.05.010

18. Ogwu AA, Darma TH, Bouquerel E (2007) Electrical resistivity of copper oxide thin films prepared by reactive magnetron sputtering. Journal of Achievements in Materials and Manufacturing Engineering 24:6

19. Lakshmanan A, Alex ZC, Meher SR (2022) Cu2O thin films grown by magnetron sputtering as solar cell absorber layers. Materials Science in Semiconductor Processing 148:. https://doi.org/10.1016/j.mssp.2022.106818

20. Minami T, Nishi Y, Miyata T (2016) Cu_2O-based solar cells using oxide semiconductors. J Semicond 37:014002. https://doi.org/10.1088/1674-4926/37/1/014002

21. Zang Z (2018) Efficiency enhancement of ZnO/Cu2O solar cells with well oriented and micrometer grain sized Cu2O films. Applied Physics Letters 112:042106. https://doi.org/10.1063/1.5017002

22. Nishi Y, Miyata T, Minami T (2013) The impact of heterojunction formation temperature on obtainable conversion efficiency in n-ZnO/p-Cu2O solar cells. Thin Solid Films 528:72–76. https://doi.org/10.1016/j.tsf.2012.09.090

23. Ievskaya Y, Hoye RLZ, Sadhanala A, et al (2016) Improved Heterojunction Quality in Cu_2O-based Solar Cells Through the Optimization of Atmospheric Pressure Spatial Atomic Layer Deposited $Zn_{1-x}Mg_xO$. JoVE 53501. https://doi.org/10.3791/53501

24. Minami T, Nishi Y, Miyata T (2013) High-Efficiency Cu_2O-Based Heterojunction Solar Cells Fabricated Using a Ga_2O_3 Thin Film as N-Type Layer. Appl Phys Express 6:044101. https://doi.org/10.7567/APEX.6.044101

25. Minami T, Nishi Y, Miyata T (2016) Efficiency enhancement using a $Zn_{1-x}Ge_x$-O thin film as an n-type window layer in Cu_2O-based heterojunction solar cells. Appl Phys Express 9:052301. https://doi.org/10.7567/APEX.9.052301

26. Minami T, Miyata T, Nishi Y (2014) Cu2O-based heterojunction solar cells with an Al-doped ZnO/oxide semiconductor/thermally oxidized Cu2O sheet structure. Solar Energy 105:206–217. https://doi.org/10.1016/j.solener.2014.03.036

27. Chen S, Wang L, Zhou C, Yang J (2023) A review of Cu2O solar cell. Journal of Renewable and Sustainable Energy 15:062701. https://doi.org/10.1063/5.0167383

28. Lakshmanan A, Alex ZC, Meher SR (2022) Recent advances in cuprous oxide thin film based photovoltaics. Materials Today Sustainability 20:. https://doi.org/10.1016/j.mtsust.2022.100244

29. Kartha CV, Rehspringer J-L, Muller D, et al (2022) Insights into Cu2O thin film absorber via pulsed laser deposition. Ceramics International 48:15274–15281. https://doi.org/10.1016/j.ceramint.2022.02.061

30. Chen Aiping PL Hua Long, Xiangcheng Li, Yuhua Li, Guang Yang* (2009) Controlled growth and characteristics of single-phase Cu2O and CuO films by pulsed laser deposition. Vaccum 83:927–930. https://doi.org/10.1016/j.vacuum.2008.10.003

31. Wang K, Gao W, Zheng HW, et al (2017) Heteroepitaxial growth of Cu2O films on Nb-SrTiO3 substrates and their photovoltaic properties. Ceramics International 43:16232–16237. https://doi.org/10.1016/j.ceramint.2017.08.205

32. Farhad SFU, Cherns D, Smith JA, et al (2020) Pulsed laser deposition of single phase n- and p-type Cu2O thin films with low resistivity. Materials & Design 193:108848. https://doi.org/10.1016/j.matdes.2020.108848

33. Lee SW, Lee YS, Heo J, et al (2014) Improved Cu2O-Based Solar Cells Using Atomic Layer Deposition to Control the Cu Oxidation State at the p-n Junction. Advanced Energy Materials 4:1301916. https://doi.org/10.1002/aenm.201301916

34. de Melo C, Jullien M, Battie Y, et al (2019) Semi-Transparent p-Cu2O/n-ZnO Nanoscale-Film Heterojunctions for Photodetection and Photovoltaic Applications. ACS Appl Nano Mater 2:4358–4366. https://doi.org/10.1021/acsanm.9b00808

35. Shenje L, Larson S, Zhao Y, Ullrich S (2020) Composition Effects on Ultrafast Optical Properties of CuxOy Thin Films: A Transient Absorption Study. J Phys Chem C 124:24908–24918. https://doi.org/10.1021/acs.jpcc.0c08716

36. Patterson AL (1939) The Scherrer Formula for X-Ray Particle Size Determination. Phys Rev 56:978–982. https://doi.org/10.1103/PhysRev.56.978

37. Reddy AS, Uthanna S, Reddy PS (2007) Properties of dc magnetron sputtered Cu2O films prepared at different sputtering pressures. Applied Surface Science 253:5287–5292. https://doi.org/10.1016/j.apsusc.2006.11.051

38. Hallberg J, Hanson RC (1970) The elastic constants of cuprous oxide. physica status solidi (b) 42:305–310. https://doi.org/10.1002/pssb.19700420131

39. Azimi H, Kuhri S, Osvet A, et al (2014) Effective Ligand Passivation of Cu2O Nanoparticles through Solid-State Treatment with Mercaptopropionic Acid. J Am Chem Soc 136:7233–7236. https://doi.org/10.1021/ja502221r

40. Ito T, Kawashima T, Yamaguchi H, et al (1998) Optical Properties of Cu 2O Studied by Spectroscopic Ellipsometry. Journal of the Physical Society of Japan 67:2125–2131. https://doi.org/10.1143/JPSJ.67.2125

41. Li J, He M, Yan J, et al (2022) Room Temperature Engineering Crystal Facet of Cu2O for Photocatalytic Degradation of Methyl Orange. Nanomaterials 12:. https://doi.org/10.3390/nano12101697

42. Ghijsen J, Tjeng LH, van Elp J, et al (1988) Electronic structure of Cu2O and CuO. Phys Rev B 38:11322–11330. https://doi.org/10.1103/PhysRevB.38.11322